Computation & theory



Phonon transport anomaly in metavalent bonded materials: contradictory to the conventional theory

Mohammed Al-Fahdi¹, Xiaoliang Zhang², and Ming Hu^{1,*} (5)

Received: 21 March 2021 Accepted: 16 September 2021 Published online:

29 September 2021

© The Author(s), under exclusive licence to Springer Science+Business Media, LLC, part of Springer Nature 2021

ABSTRACT

We report a phenomenon occurring in some chalcopyrite structures with space group $R\overline{3}m$ (space group number: 166) where heavier mean atomic mass does not necessarily lead to lower lattice thermal conductivity, in contradiction to the conventional Keyes' theory of an inverse relation between lattice thermal conductivity and heavier elements. The lattice thermal conductivity is calculated for three chalcopyrite structures, namely TlBiS2, TlBiSe2, and TlBiTe2, at room temperature using phonon Boltzmann transport equation with interatomic force constants evaluated by density functional theory (DFT). According to Keyes' theory, the decedent order of lattice thermal conductivity should follow: TlBiS₂ > TlBiSe₂ > TlBiTe₂. However, our first-principles calculations demonstrate that TlBiSe₂ has higher lattice thermal conductivity than TlBiS₂, although the Se atoms are heavier than S atoms. Resorting to full first-principles calculations, we reveal the relatively lower lattice thermal conductivity of TlBiS₂ compared to TlBiSe₂ originates from the largely suppressed phonon relaxation time, in particular for optical phonons, which negatively affects thermal transport, although both heat capacity and phonon group velocity of TlBiS₂ are higher than that of TlBiSe2, which should have led to higher lattice thermal conductivity in TlBiS₂. Detailed analysis of phonon partial density of states (PDOS) demonstrates that the short phonon relaxation time in TlBiS₂ is due to the extensive strongly anharmonic phonon interactions solely associated with the vibrations of S atoms as shown in PDOS, which reduces the life of the phonon transport in TlBiS2, while in TlBiSe2 and TlBiTe2 the thermally conductive collective modes are present. The higher anharmonic phonon-phonon interactions are also attributed to the higher transferred charges present in TlBiS₂. We also provide a microscopic picture connecting the strong phonon anharmonicity to the stereo-chemically lone-pair electrons present in the chalcopyrite structures. Moreover by analyzing the atomic charges, our calculations

Handling Editor: Avinash Dongare.

Address correspondence to E-mail: hu@sc.edu



¹ Department of Mechanical Engineering, University of South Carolina, Columbia, SC 29208, USA

²Key Laboratory of Ocean Energy Utilization and Energy Conservation of Ministry of Education, School of Energy and Power Engineering, Dalian University of Technology, Dalian 116024, China

show that these materials possess a recently discovered new type of bonding named metavalent bonding, which is featured by giant phonon anharmonicity, high transverse optical Grüneisen parameters, high Born effective charges, and high dielectric constants. These results provide deep understanding of metavalent bonding induced unusual heat transfer mechanism and offer a new route to designing novel materials with ultralow lattice thermal conductivity, which is extremely attractive for waste-heat recovery (thermoelectrics) and thermal insulation applications.

Introduction

Heat transfer is one of the dominant forms of energy transfer. Manipulating the thermal transport process in materials is useful in many real applications which can be represented by two opposing aspects: On the one hand, materials with high thermal conductivity that dissipate the accumulated heat in electronic devices in thermal management applications to extend the lifetime of those devices [1-3]. On the other hand, low thermal conductivity materials are desired in thermoelectric applications along with high electrical conductivity, Seebeck coefficient to achieve high thermoelectric figure of merit [4, 5]. In quantum scale studies, phonons play an important role in the heat transport process [6, 7]. According to the simple kinetic theory and linearized Boltzmann transport equation (BTE), lattice thermal conductivity (k_L) is calculated by the summation of all the phonon modes as

$$k_L = \sum_{\lambda} c_{\lambda} \tau_{\lambda} \Lambda_{\lambda} = \sum_{\lambda} c_{\lambda} v_{\lambda} \tau_{\lambda}^2 \tag{1}$$

where $v_{\lambda} = \frac{\Lambda_{\lambda}}{\tau_{\lambda}}$, λ denotes a specific phonon mode, c is the volumetric heat capacity, Λ is the mean free path (MFP), τ is the phonon relaxation time, and v is the phonon group velocity [6, 7]. From this equation, we find that the lattice thermal conductivity of a crystalline material is contributed by various parameters at each mode, i.e., the volumetric heat capacity, phonon relaxation time, group velocity, and mean free path, which makes analysis of the dominant parameter contributing to the lattice thermal conductivity extremely challenging.

Moreover, the dependence of lattice thermal conductivity on physical and/or chemical properties is complicated, which makes the task of correlating lattice thermal conductivity to other macroscopic

chemical or physical properties a complicated task. According to the Keyes' expression, higher mean atomic mass yields lower lattice thermal conductivity [8]. This trend holds true in the case of diamond-like structures with $Fd\overline{3}m$ symmetry (space group number: 227) of group (IVA) where carbon (C) which is the lightest diamond-like structure has the highest lattice thermal conductivity of 2,200 W/mK, silicon (Si) has a lattice thermal conductivity of $\sim 150 \text{ W}/$ mK, and germanium (Ge) which has the heaviest diamond-like structure in the comparison has the lowest lattice thermal conductivity of 60 W/mK [9]. The trend was also seen in binary, ternary, and chalcopyrite materials [9–11]. However, not all materials follow this rule. For instance, recent study found that binary CaO has lower lattice thermal conductivity compared to CaS [10], despite of lighter mass of oxygen (O) than sulfur (S). The phenomenon was also seen in chalcopyrite structures that have the formula of ABC2 which confirmed that CuAlS2 has a lower lattice thermal conductivity compared to that of CuAlSe₂ and CuAlTe₂ [11]. However, the underlying mechanism that materials with heavier elements have lower lattice thermal conductivity than those of lighter elements is not well understood to date.

Three chalcopyrite structures, namely TlBiS₂, TlBiSe₂, and TlBiTe₂, were studied in the literature for having lone-pair electrons [12, 13], but it was never reported how the lone-pair electrons affect the strong anharmonicity in those structures. For instance, the in-plane lattice thermal conductivity of TlBiSe₂ was found to be 0.82 W/mK and its cross-plane lattice thermal conductivity is 0.87 W/mK [14]. Here, we systematically calculated the lattice thermal conductivity of TlBiSe₂, TlBiSe₂, and TlBiTe₂ to discover potential anomalous results in lattice thermal conductivity among the three materials and prove the



effect of lone-pair electrons on the ultralow thermal conductivity. Moreover, we discover that all these materials have metavalent bonding, which is known for its pronounced phonon anharmonicity [15, 16]. The mechanism of metavalent bonding induced anomalous trend in heavier elements not necessarily leading to lower thermal conductivity is thoroughly explored and investigated from electronic structure point of view. The results gained through this study unravel a new physics about phonon transport in metavalent bonded materials which will help designing exceptional candidate materials to be used in thermoelectric applications [15, 16].

Computational methods

For the chalcopyrite materials studied herein the initial atomic structure files of TlBiS2, TlBiSe2, and TlBiTe₂ were obtained from Materials Project (MP) database. The materials with their corresponding IDs are TlBiS₂ (mp-554310), TlBiSe₂ (mp-29662), and TlBiTe₂ (mp-27438) with the same space group $R\overline{3}m$ (space group number: 166) [17]. The materials have the following band gaps: 0.553 eV, 0.347 eV, and 0.415 eV for TlBiS₂, TlBiSe₂, and TlBiTe₂, respectively [17]. Since the materials are semiconductors, thermal conductivity contributed from phonons was considered in this study because phonons play the dominant role in the thermal transport process of semiconductors (for most of undoped states) and insulators. First-principles calculations were performed using Vienna ab initio simulation package (VASP) based on density functional theory (DFT) [18–20]. The Perdew-Burke Ernzerhof (PBE) [21] of the generalized gradient approximation (GGA) is chosen as the exchange-correlation functional. The electronic wavefunctions projector augmented wave method (PAW) modeling with a kinetic energy cutoff of 400 eV was used [20, 22]. The Brillouin zone was sampled with Monkhorst-pack [23] k-mesh of $10 \times 10 \times 10$. The structures were relaxed with 10^{-7} eV and 10^{-4} eV/Å as energy and force convergence criteria, respectively. During the optimization process, the unit cell could change its size, and the atoms could move until each of the convergence criteria mentioned previously were met. Born effective charge (BEC) (Z^*) and dielectric constant (ε) were calculated using density functional perturbation theory (DFPT).

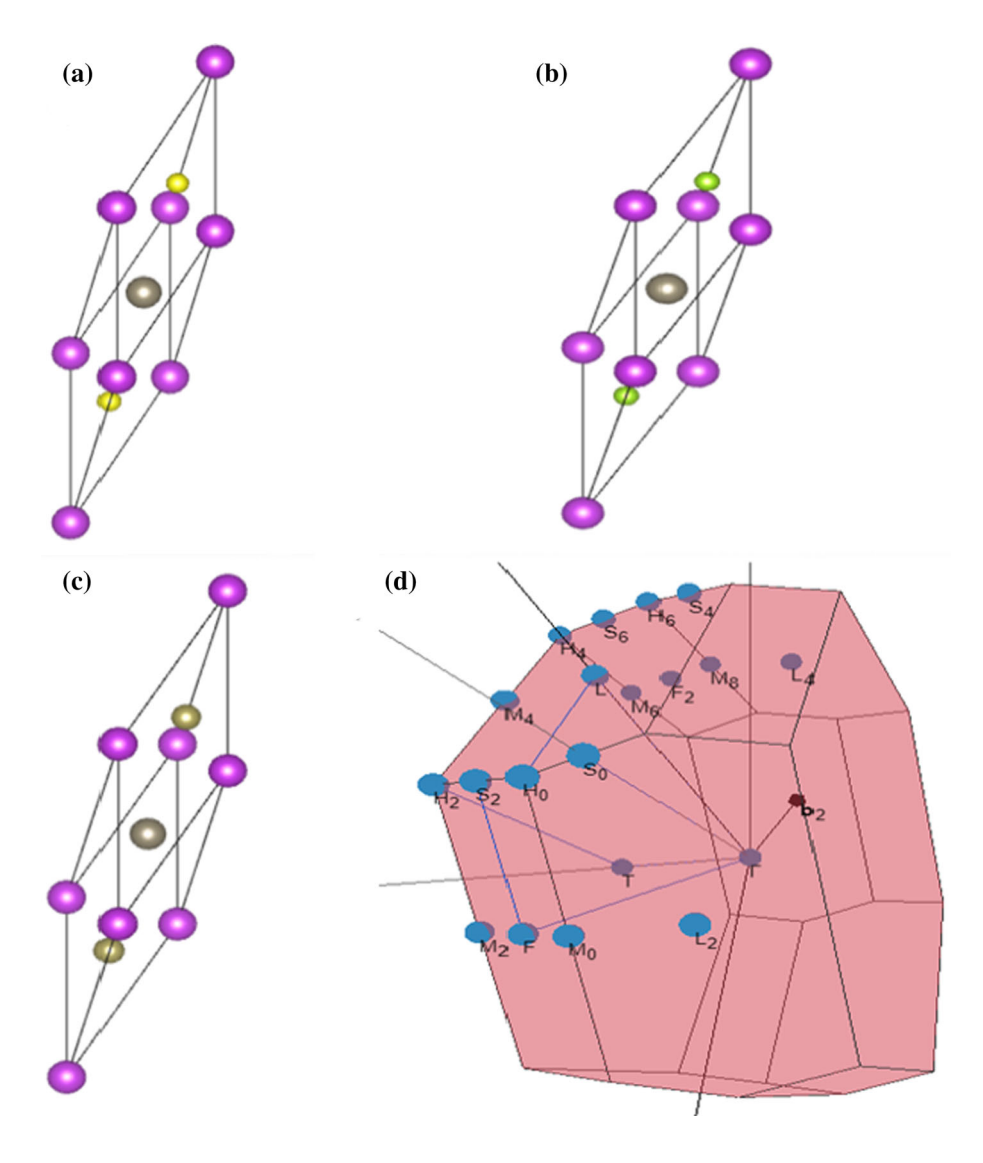
The transferred and shared charges were calculated by density-derived electrostatic and chemical (DDEC6) method [24–26]. The transferred charge was directly extracted from the Chargemol package [27] and reported as it was shown in the files. Shared charges were calculated by multiplying the original values by a factor of two considering the original values represent the delocalization indices and shared charges are twice their delocalization indices.

A supercell of $2 \times 2 \times 2$ was created for all materials, and the harmonic second-order interatomic force constants of the supercells were calculated by the finite displacement method using PHONOPY [27]. In the finite displacement method, PHONOPY code calculated the dynamical matrix in reciprocal space from the energy derivatives to obtain the phonon dispersion of each supercell, from which the phonon group velocities were calculated. Phonon group velocity of each phonon mode was also calculated by PHONOPY. Two more supercells (1% larger and 1% smaller in size) for each material were created to calculate the Grüneisen parameter at each phonon mode and then the phonon dispersions were color-mapped by the magnitude of the Grüneisen parameter values at each mode. The Grüneisen parameter calculation included the effect of longitudinal optical-transverse optical (LO-TO) splitting from the dielectric tensor and Born effective charges calculated by DFPT.

Phonon relaxation time, phase space, and lattice thermal conductivity were calculated by linearized Boltzmann transport equation (BTE) as it was solved iteratively by the ShengBTE package [28] which used the second harmonic interatomic force constants from PHONOPY and third-order anharmonic interatomic force constants calculated by the ShengBTE package. This technique has been widely used for predicting phononic thermal transport in various materials in the past few years [29-32]. The third-nearest-neighbor interactions with q-point grid of $16 \times 16 \times 16$ were taken into consideration when calculating the lattice thermal conductivity by the ShengBTE package. We have carefully tested the convergence of q-point grid and found that the average thermal conductivity results difference between q-point grid of $12 \times 12 \times 12$ and $16 \times 16 \times 16$ is less than 0.01 W/mK.



Figure 1 Crystal structure of a TlBiS₂: Tl (dark brown), Bi (purple), S (yellow), b TlBiSe₂: Tl (dark brown), Bi (purple), Se (green), and c TlBiTe₂: Tl (dark brown), Bi (purple), Te (light brown). d Corresponding Brillouin zone with different labeled paths for structures with space group $R\overline{3}m$ (space group number: 166).



Results and discussion

The crystal structures for the three materials are shown in Fig. 1 in which the atoms are identified by different colors. The crystal structures were imported from VESTA code [33]. Figure 1a shows the crystal structure of TlBiS₂, Fig. 1b shows the crystal structure of TlBiSe2, and Fig. 1c shows the crystal structure of TlBiTe₂. Figure 1d shows the corresponding Brillouin zone with different high symmetry paths in which some will be used to calculate the phonon dispersions. The high symmetry paths were calculated by the SeeK path package [34]. All three materials have the same high symmetry paths due to them having group $R\overline{3}m$ space same (space number = 166).

Lattice thermal conductivity reported here for all three chalcopyrite materials are calculated at 300 K. The average lattice thermal conductivity results are as follows: 0.8826 W/mK for TlBiS₂, 0.9383 W/mK for TlBiSe₂, 0.2841 W/mK for TlBiTe₂. Lattice thermal conductivity is higher in TlBiSe2 than TlBiS2 as calculated by DFT. These results are anomalous to Keyes' rule which indicates the inverse relationship between thermal conductivity and mean atomic mass [8] which was also confirmed by Slack's model [35]. Heavier elements flatten the phonon dispersion which reduces the lattice thermal conductivity [36] by increasing the number of the phonon scattering channels in the phase space, and decreasing group velocity, decreasing phonon relaxation time [7], and scattering more phonons [37]. Therefore, according to Keyes' rule, TlBiS₂ should have a higher lattice



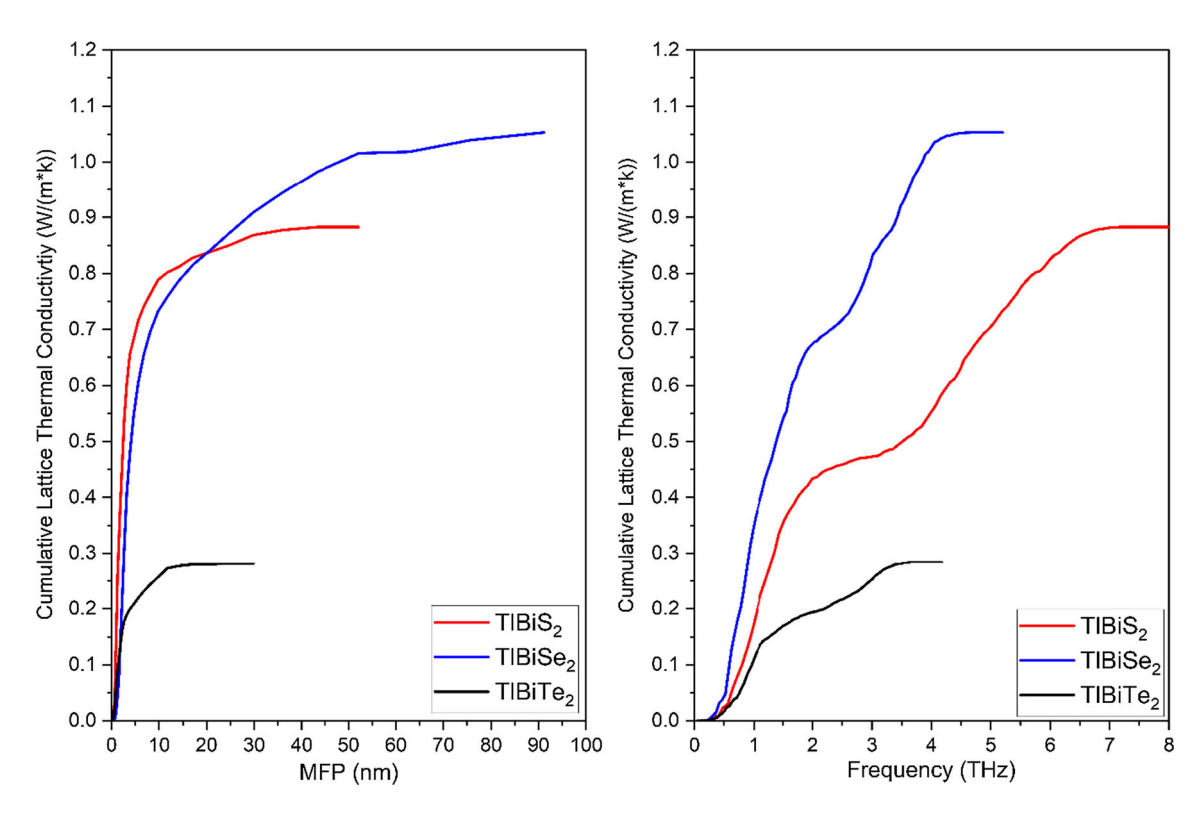


Figure 2 a Cumulative lattice thermal conductivity vs. mean free path (MFP); b Phonon frequency dependent cumulative lattice thermal conductivity.

thermal conductivity. The anomaly that the heavier elements do not always have higher thermal conductivity, as calculated by DFT in this paper, was also confirmed by experiments in some other materials [11, 38–40]. DFT was able to discover similar anomalies of lattice thermal conductivity with mean atomic mass in some other materials [10, 41].

Figure 2 shows (a) accumulative lattice thermal conductivity with mean free path (MFP) and (b) cumulative lattice thermal conductivity with respect to frequency for all three materials. As seen from Fig. 2a, the rule that lattice thermal conductivity is higher with lighter mean atomic mass holds true between TlBiS2 and TlBiSe2 for MFP up to 20 nm, beyond which the lattice thermal conductivity of TlBiSe₂ keeps rising and finally overwhelms TlBiS₂ significantly. For TlBiTe2 the thermal conductivity is largely suppressed for MFP below 10 nm, as compared with TlBiS₂ and TlBiSe₂. Figure 2 suggests that TlBiS₂ has less phonons that contribute to increasing lattice thermal conductivity at higher MFP than TlBiSe₂. The reason for that is due to TlBiS₂ having higher phonon-phonon interactions which decrease the contribution of phonons with higher MFP (equals group velocity multiplied by phonon relaxation time). More on phonon–phonon interactions is in "Insight from Lone-Pair Electrons and Phonon Anharmonicity" section. As for Fig. 2b, the mode frequency-dependent accumulative lattice thermal conductivity is plotted with respect to frequency which also confirms the anomaly between TlBiS₂ and TlBiSe₂, since TlBiSe₂ has higher lattice thermal conductivity across all the frequency range of both materials.

Figure 3 shows the phonon frequency-dependent accumulative lattice thermal conductivity along each direction of TlBiS₂, TlBiSe₂, and TlBiTe₂. The anomaly holds true in all three directions as seen in Fig. 3 when comparing the lattice thermal conductivity of each direction in each structure. However, one note to consider in these plots is the significant contribution from optical phonons to the total lattice thermal conductivity, which is due to the high group velocity in the optical phonon branches in the phonon dispersion plots of the three materials. Group velocity will be discussed in a later part in the results discussion. A noticeable feature in Fig. 3 is the flat plateau in the middle frequency range (about 2.5 THz -4.5 THz) for TlBiS₂, while such plateau gradually disappears for TlBiSe2 and TlBiTe2. This plateau is



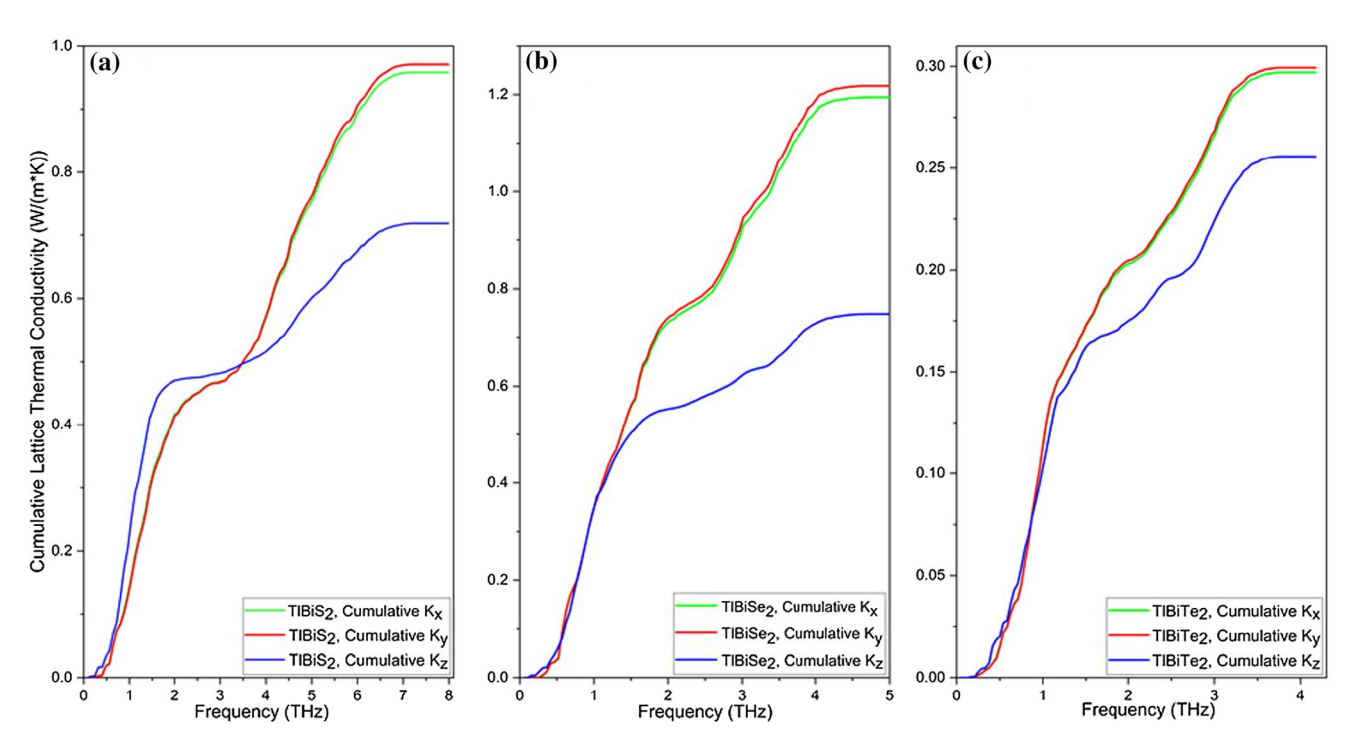


Figure 3 Cumulative lattice thermal conductivity of a TlBiS₂, b TlBiSe₂, and c TlBiTe₂ with respect to frequency at 300 K in each direction.

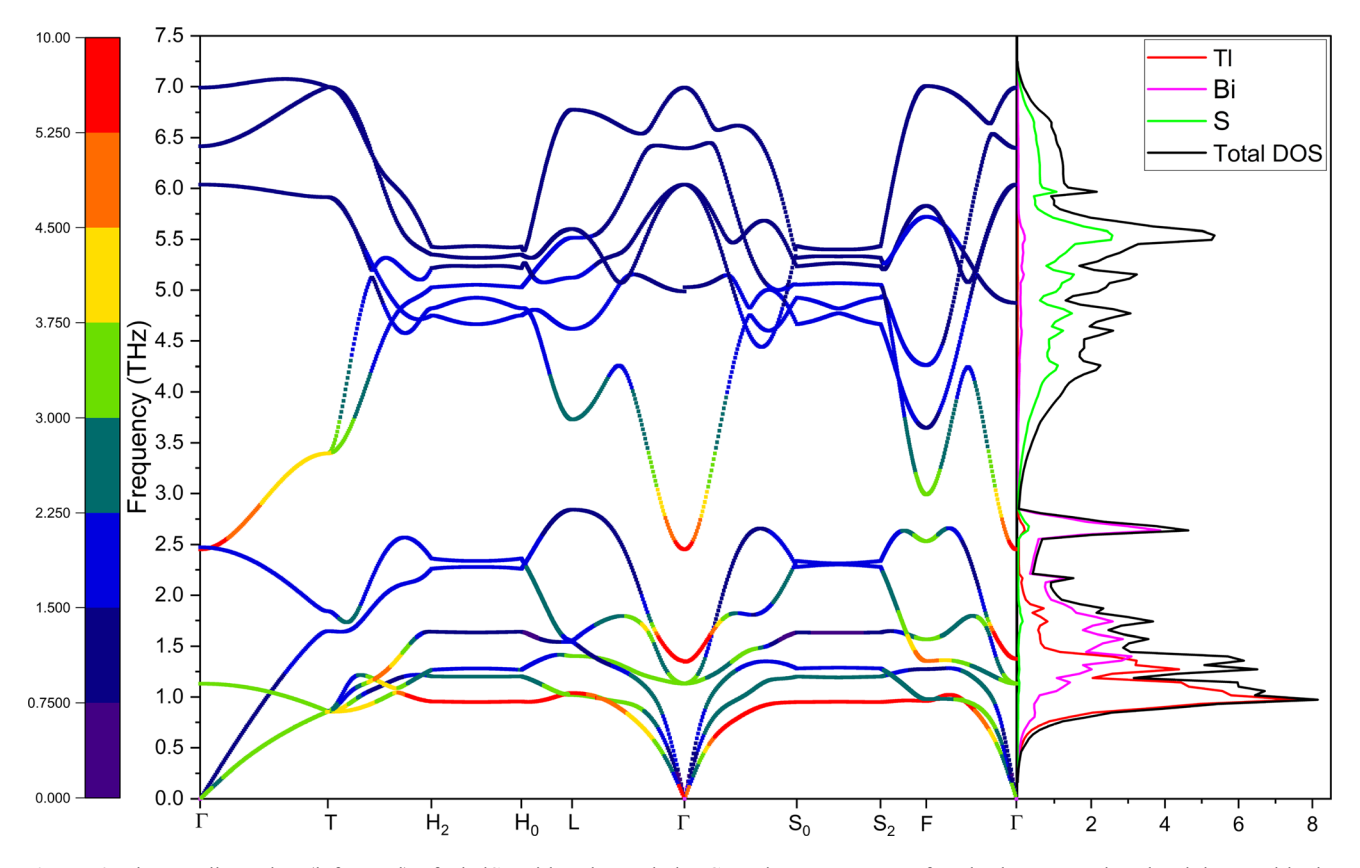


Figure 4 Phonon dispersion (left panel) of $TlBiS_2$ with color code by Grüneisen parameter of each phonon mode. The right panel is the partial density of states (PDOS) and total DOS.



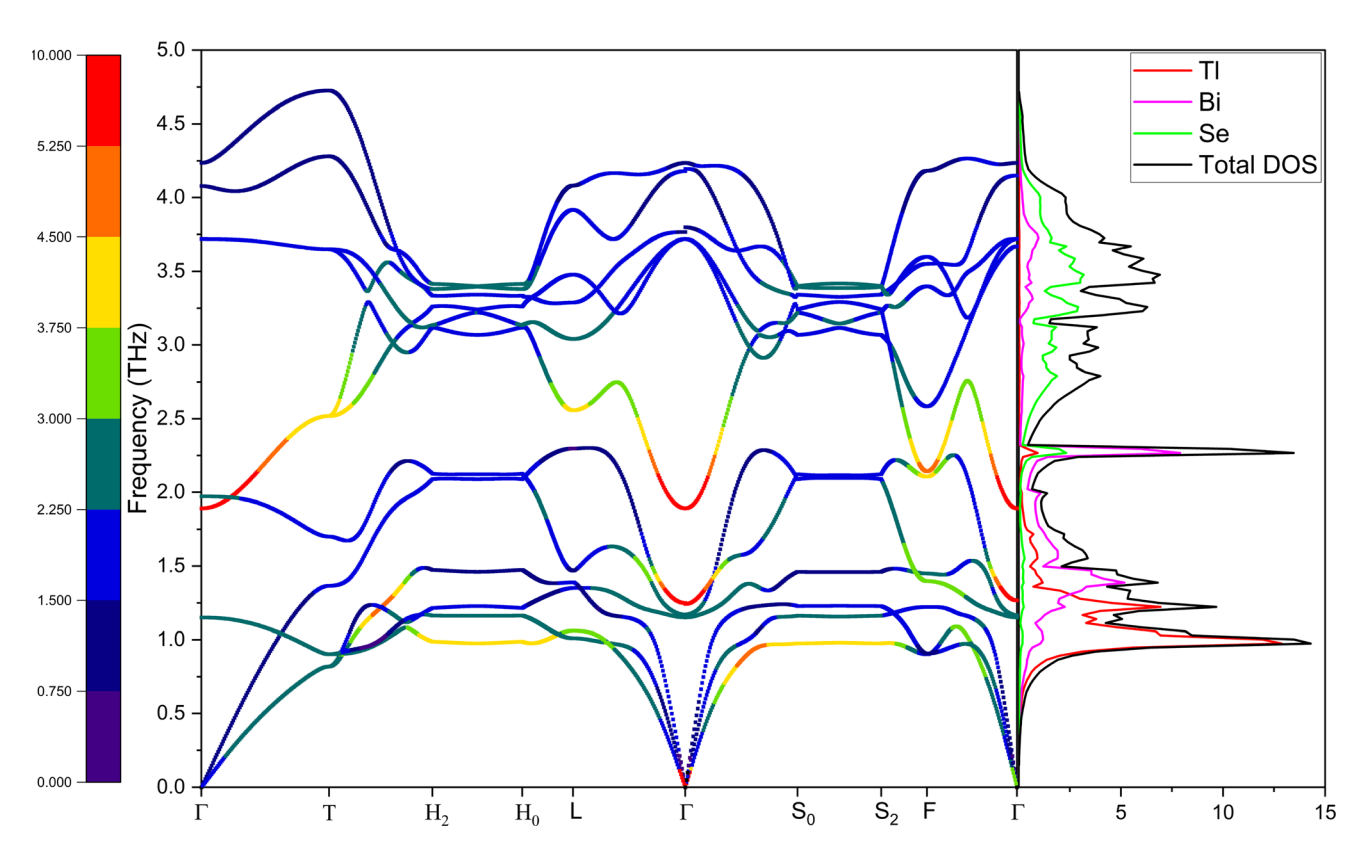


Figure 5 Phonon dispersion (left panel) of TlBiSe₂ with color code by Grüneisen parameter of each phonon mode. The right panel is the partial density of states (PDOS) and total DOS.

solely due to the fewer phonon modes existing in this frequency range (see more details in the phonon dispersions plots in Figs. 4, 5, and 6).

The phonon dispersions of TlBiS₂,TlBiSe₂, and TlBiTe₂ with color scale represented by Grüneisen parameter at each phonon mode are shown in the left panel of Figs. 4, 5, and 6, respectively. The phonon partial density of states (PDOS) for each material are also shown in the right panel of corresponding figures. All phonon dispersions do not have negative frequency which indicates thermodynamical stability in all three materials [10, 41-43]. TlBiS₂ has the highest range of phonon frequencies up to \sim 7 THz, while TlBiSe2 has the second-highest phonon frequencies (up to ~ 4.75 THz), and TlBiTe₂ has the lowest phonon frequency range (up to ~ 3.75 THz). Overall, the shapes of the phonon dispersions for the three materials look vastly similar, considering their immensely comparable structures and analogous interatomic force constants. However, distinct difference is found in colored Grüneisen parameter, especially for the two transverse acoustic (TA) phonon modes coming out from the Γ -point. For TlBiS₂, large Grüneisen parameter values are found in these TA modes, e.g., along the $\Gamma \rightarrow L \rightarrow H_0 \rightarrow H_2$ path and $\Gamma \to S_0 \to S_2 \to F$ path. This is the solid evidence for the strong phonon anharmonicity in TlBiS₂ as compared with TlBiSe2 and TlBiTe2. Another important difference resides in the high frequency PDOS. For TlBiS₂, the PDOS above the frequency of ~ 4 THz is solely contributed by the vibrations of S atoms, while for TlBiSe₂ the Bi atoms also contribute partially to the total PDOS in the high-frequency range and for TlBiTe2 the Bi atoms have even larger contribution. This implies that, there are intense highfrequency phonon-phonon interactions prevailing in TlBiS₂. Such phonon modes usually possess short phonon relaxation time as we will see later in the work.

Different phonon frequency range indicates that there is a large overlap in the phonon modes in the following order $TlBiTe_2 > TlBiSe_2 > TlBiSe_2$, which also confirms that the total phase space (P_3) is higher in the materials with smaller phonon bandgaps [7, 44]. High total phase space refers to more three-phonon scattering channels [7, 44]. To have an



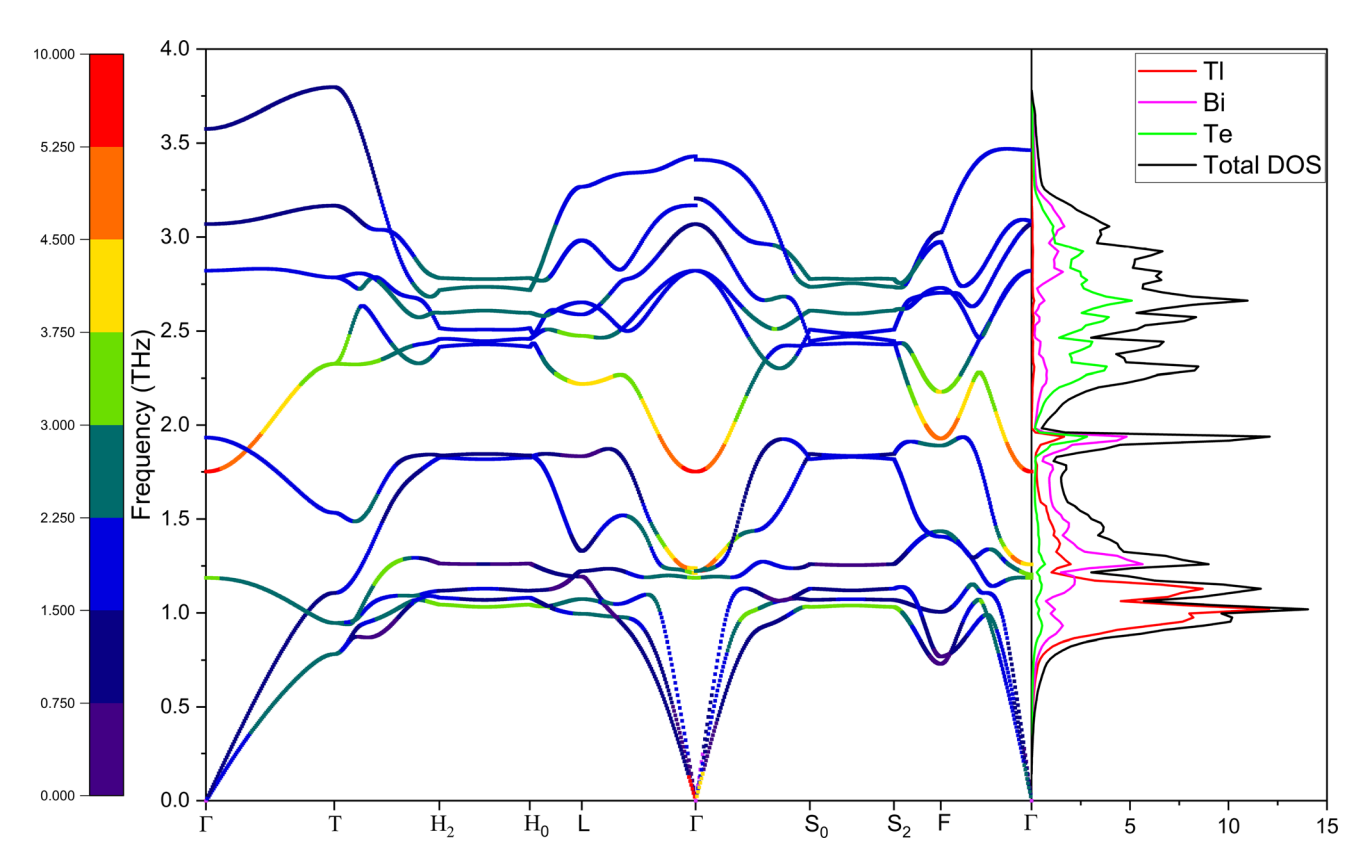


Figure 6 Phonon dispersion (left panel) of TlBiTe2 with color code by Grüneisen parameter of each phonon mode. The right panel is the partial density of states (PDOS) and total DOS.

introductory understanding of the three-phonon scattering, the phase space is determined by integration of conservation conditions of energy and momentum δ -functions [45]:

$$\omega_{i}(q) \pm \omega_{i'}(q') = \omega_{i''}(q''), q \pm q' = q'' + G$$
 (2)

where $\omega_i(q)$ is the frequency of a specific phonon mode, (j,q) are phonon branch and momenta of a phonon, respectively, and G is the reciprocal lattice vector which is equal to zero in the case of Normal process and non-zero for the Umklapp processes. The sign ± depends on the type of three-phonon processes [46]. To quantify three-phonon scattering phase space [10, 47]:

$$P_3 = \frac{2}{3\Omega} \left(P_3^{(+)} + \frac{1}{2} P_3^{(-)} \right) \tag{3}$$

where
$$P_3^{(\pm)} = \sum_i \int dq D_j^{(\pm)}(q)$$
 and

where
$$P_3^{(\pm)} = \sum_j \int \!\! dq D_j^{(\pm)}(q) \qquad \text{and}$$

$$D_j^{(\pm)}(q) = \sum_{j'j''} \int \!\! dq' \delta(\omega_j(q) \pm \omega_{j'}(q') - \omega_{j''}(q \pm q'' - G)), \; \Omega$$

is the normalization factor, $D_i^{(\pm)}(q)$ is the two phonon density of states and momentum conservation which

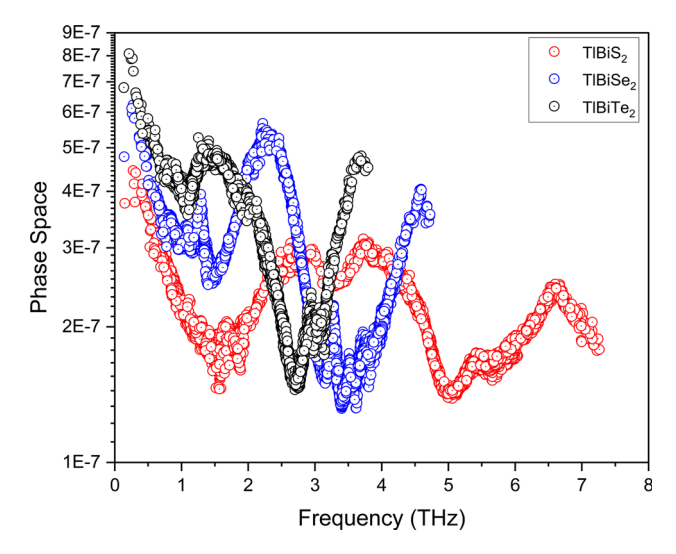


Figure 7 Comparison of frequency dependent log scaled phase space in TlBiS₂, TlBiSe₂, and TlBiTe₂.

is imposed on q'' [48]. P_3 is used to assess the number of scattering events that satisfy the conservation conditions of the scattering channels at each phonon mode. As a result, P_3 is inversely proportional to the lattice thermal conductivity [49, 50].



The phase space is the highest in TlBiTe₂ as shown in Fig. 7, due to the aforementioned large overlap of optical phonons with the acoustic phonons (no obvious phonon band gap in Fig. 6). TlBiSe₂ has the second-highest phase space shown in Fig. 7 and the second-highest overlap between acoustic phonons with the optical phonons as shown in Fig. 5. TlBiS₂ has the smallest phase space, in particular for the low-frequency range (< 1.5 THz) and the least overlap between acoustic phonons branch with the optical phonons branch as seen in Fig. 4. Phase space also indicates that TlBiTe₂ has more three-phonon scattering channels than TlBiSe₂ and TlBiS₂ in which TlBiS₂ has the lowest three-phonon scattering channels (Table 1).

To analyze lattice thermal conductivity, each parameter in Eq. (1) must be analyzed. The volumetric heat capacity is the simplest parameter in Eq. (1). Table 1 shows the values of the volumetric heat capacity, lattice thermal conductivity in each direction, and total phase space to give a short summary of the values discussed previously.

The results of total phase space and volumetric heat capacity presented in Table 1 suggest that TlBiS₂ would have higher lattice thermal conductivity which would also support Keyes' rule since it has higher volumetric heat capacity and lower total phase space, but the final lattice thermal conductivity results from DFT calculation show the opposite results to that predicted by Keyes' rule. Moreover, the lattice thermal conductivity results show the anomaly in all directions i.e., the lattice thermal conductivity is higher in TlBiSe₂ as compared to TlBiS₂ in x, y, and z directions. Obviously, the volumetric heat capacity and total phase space cannot explain the relatively lower lattice thermal conductivity of TlBiS₂ compared to that of TlBiSe₂.

The second factor of lattice thermal conductivity in Eq. (1) is the group velocity. Figure 8 shows the phonon group velocity at each phonon mode in (a) TlBiS₂, (b) TlBiSe₂, and (c) TlBiTe₂. The group

velocity is calculated as the slope of phonon dispersions, i.e., $v = \frac{\partial \omega}{\partial k}$ (the slope of frequency with respect to wavenumber). Group velocity is represented by the color bar on the right side of Fig. 8. The same standard of group velocity color bar is implemented on (a) TlBiS₂, (b) TlBiSe₂, and (c) TlBiTe₂ which is between 0 and 35 Å/ps. In this way, we can distinguish the group velocity on the same phonon modes among all three materials and determine which phonon modes have higher group velocity. The phonon group velocity is higher in TlBiS2 followed by TlBiSe₂ then TlBiTe₂ which is also predicted from the phonon dispersion plots in Figs. 4, 5 and 6 since the slope of TlBiS₂ bands is higher than that of TlBiSe₂ followed by TlBiTe₂. Also, TlBiS₂ has the highest band frequency followed by TlBiSe2 then TlBiTe₂ which is consistent with having higher slopes of frequency with respect to the wavenumber in the phonon dispersion plots and consequently higher group velocity in TlBiS2, TlBiSe2, then TlBiTe2. One important note in Fig. 8 is the abnormally high group velocity in the optical phonon branch especially in TlBiS₂ which contributes significantly to the overall lattice thermal conductivity shown in Fig. 2. The group velocity also indicates that TlBiS₂ should have higher lattice thermal conductivity than that of TlBiSe₂. Again, the phonon group velocity cannot explain the relatively lower thermal conductivity of TlBiS₂ when compared to TlBiSe₂.

The last parameter of lattice thermal conductivity is the phonon relaxation time. In Fig. 9, we compare the mode level phonon relaxation time for the three materials. Generally, for all three materials, the phonon relaxation time values drop after the acoustic branch phonon modes where the Grüneisen parameter is high in all phonon dispersions as shown in Figs. 4, 5 and 6. Also, those phonon modes with low phonon relaxation time and high Grüneisen parameter have small contribution to the total lattice thermal conductivity seen in Fig. 3 which confirms the inverse relationship between lattice thermal

Table 1 Volumetric heat capacity, lattice thermal conductivity in each direction, and total phase space of TlBiS₂, TlBiSe₂, and TlBiTe₂

Chalcopyrite materials	Volumetric heat capacity at 300 K (kJ/K m³)	$\kappa_{xx}(W/mK)$	$\kappa_{yy}(W/mK)$	$\kappa_{zz}(W/mK)$	Total phase space
TlBiS ₂	1,443	0.9583	0.9709	0.7187	0.01012
TlBiSe ₂	1,326	1.0137	1.0264	0.7747	0.01354
TlBiTe ₂	1,131	0.2970	0.2994	0.2558	0.01597



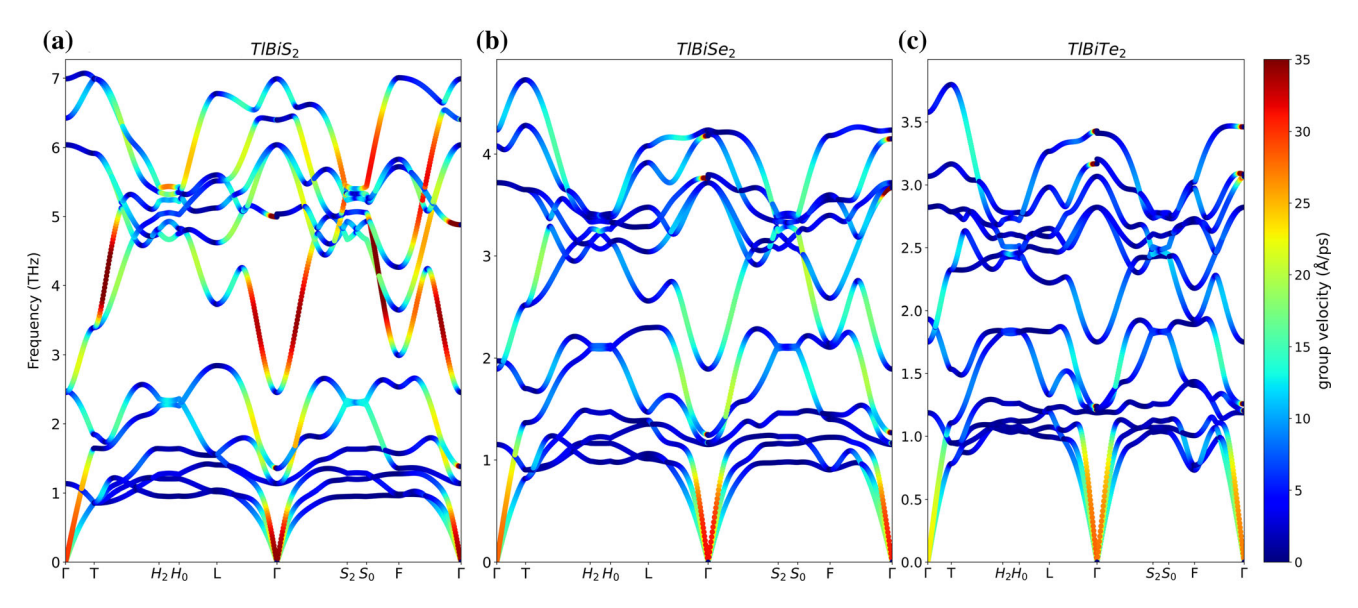


Figure 8 Phonon dispersion of a TlBiS₂, b TlBiSe₂, and c TlBiTe₂ with group velocity for each phonon mode represented by a standard color bar on the right with the same scale (0–35) Å/ps.

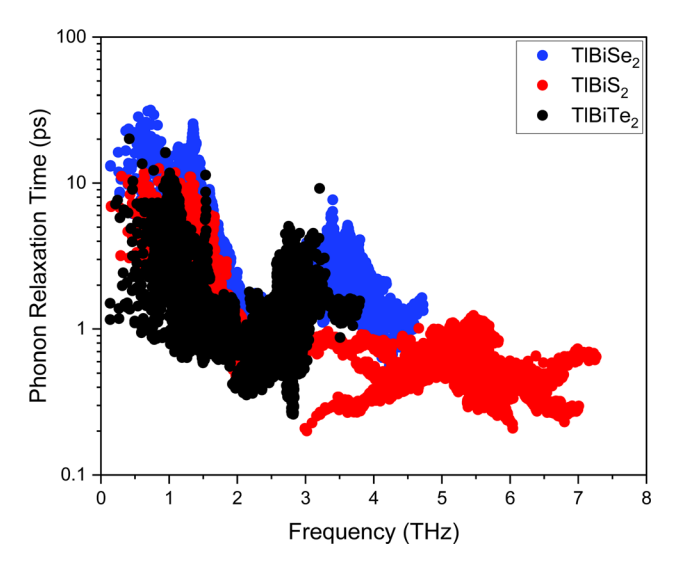


Figure 9 Frequency dependent log scaled phonon relaxation time of TlBiS₂, TlBiSe₂, and TlBiTe₂.

conductivity and Grüneisen parameter [51]. Overall, the phonon relaxation time of TlBiS₂ in the entire frequency range is significantly lower than that of TlBiSe₂, which explains the trend of its lower lattice thermal conductivity, despite of of TlBiS₂ having higher heat capacity and group velocity. Certainly, it is no wonder why TlBiTe₂ has the lowest phonon relaxation time, resulting in the lowest lattice thermal conductivity among the three materials. Interestingly enough, the phonon relaxation time for TlBiS₂ at high-frequency range (> 3 THz) is extremely low, indicating strong phonon anharmonicity of these

modes. This result is consistent with previous analysis to the high-frequency PDOS in Fig. 4, which shows strongly localized phonon modes (solely contributed by the S atoms). Now, we understand that the abnormally lower lattice thermal conductivity of TlBiS₂ than that of TlBiSe₂ stems from the unexpectedly shorter phonon relaxation time, which mainly occur in these high-frequency phonon modes. Phonon relaxation time values increase significantly in TlBiSe₂ and TlBiTe₂ in the optical phonon branch, but that is not the case for TlBiS₂ which has the lowest phonon relaxation time in the optical phonon branch.

As a short summary of the abnormal results, the volumetric heat capacity, total phase space, and group velocity indicate that TlBiS₂ would have higher lattice thermal conductivity supporting Keyes' rule. However, the phonon relaxation time is substantially shorter in TlBiS₂, specifically, in the optical branch than the other two materials, which makes TlBiS₂ have lower lattice thermal conductivity. The anomalous behavior of shorter phonon relaxation time in TlBiS₂ demonstrates the existing anomaly with lattice thermal conductivity in the material compared to TlBiSe₂ and TlBiTe₂.

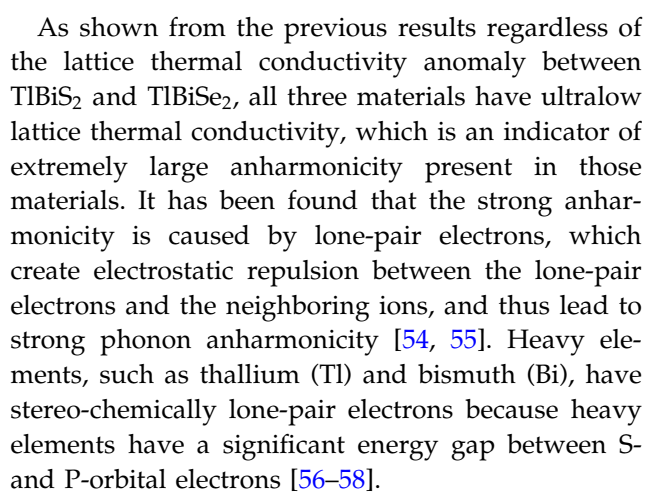


Insights from lone-pair electrons and phonon anharmonicity

It was reported that larger charge transfer usually induces larger phonon-phonon interactions [41]. Also, a previous study reported that materials with covalent bonding have higher thermal conductivity compared to ionic bonded materials [52] which also confirms that inverse relationship between transferred charges and ionic bonding with lattice thermal conductivity. The phenomenon where transferred charges yield lower lattice thermal conductivity was also seen in Ref. [53]. The phonon-phonon interactions reduced the number of phonons with higher MFP which was shown in Fig. 2a. The charge transfer is in this sequence: TlBiS₂ > TlBiSe₂ > TlBiTe₂, which results in higher phonon interactions in TlBiS₂. The larger phonon interactions yield shorter phonon relaxation time in TlBiS2 and lower number of phonons with high MFP. In this work, we add that transferred charge is one of the parameters that determine the lattice thermal conductivity by increasing the phonon–phonon interactions [41], but in most cases, the mean atomic mass would usually be a better descriptor for estimating the lattice thermal conductivity which was formulated by Keys' rule in 1959 [8] and followed by Slack in 1973 [35]. It has already been well-known that mean atomic mass negatively affects many parameters of lattice thermal conductivity by flattening the phonon dispersion plot [36] which decreases group velocity [7], increases phase space [7], and scatter more phonons [37]. For all those reasons, mean atomic mass has been successfully used to predict the trend of relative lattice thermal conductivity with some rare exceptions in which we referred to one exception in the current work. Table 2 presents the charge transfer results in the three materials.

Table 2 Comparison of transferred charges in TlBiS₂, TlBiSe₂, and TlBiTe₂

Chalcopyrite materials	Transfe	Transferred charge of each element			
	Tl	Bi	S / Se / Te		
TlBiS ₂	0.53	0.95	- 0.74		
TlBiSe ₂	0.49	0.77	-0.63		
TlBiTe ₂	0.42	0.56	-0.49		



The existence of the lone-pair electrons can be demonstrated by the electron localization function (ELF) which is computed in VASP and outputted in a file named "ELFCAR" which represent the probability (between 0-1 as shown in the color bar) of an electron locating at a certain grid. Figure 10 plots were extracted from [001] plane with an isosurface value of 0.01. Figure 10 shows the lone-pair electrons effect of repulsion between the lone-pair electrons and the neighboring atoms. The images in Fig. 10 were imported from VESTA Software [33] which shows the ELFCAR files from the discussed materials. The images show where the lone-pair electrons can be seen clearly in the three materials. In Fig. 10a the lone-pair electrons in TlBiS2 manifest as a "mushroom"-like ELF shape in Tl, while in Fig. 10b the lone-pair electrons in TlBiSe₂ have the "crescent"like ELF shape in Bi and in Fig. 10c the lone-pair electrons in TlBiTe2 have the "crescent"-like ELF shape in Bi as well. The stereo-chemically lone-pair electrons cause anharmonicity in those materials through the electrostatic repulsion between the lonepair electrons in Bi atom and the surrounding atoms, which explains the space between the lone-pair electrons in the Bi atom and the surrounding atoms as shown in Fig. 10.

Stereo-chemically active lone-pair electrons have another effect besides phonon anharmonicity, which is polarization [54]. Table 3 shows the large polarization in TlBiS₂, TlBiSe₂, and TlBiTe₂. The polarization is the highest in TlBiTe₂, which indicates that the dielectric constant and the Born effective charges are the highest in it as well, which will be seen in the following section. The large polarization values induced by lone-pair electrons in these materials are indicators of large dielectric tensors and high Born



Figure 10 Contour of the electron localization function (ELF) with isosurface value of 0.01 and along [001] plane for a TlBiS₂ with 1 Å from the origin, b TlBiSe₂ with 2.3 A from the origin, and c TlBiTe₂ with 1.4 Å from the origin. The ELF value in the contour is also labeled from 0 to 1.

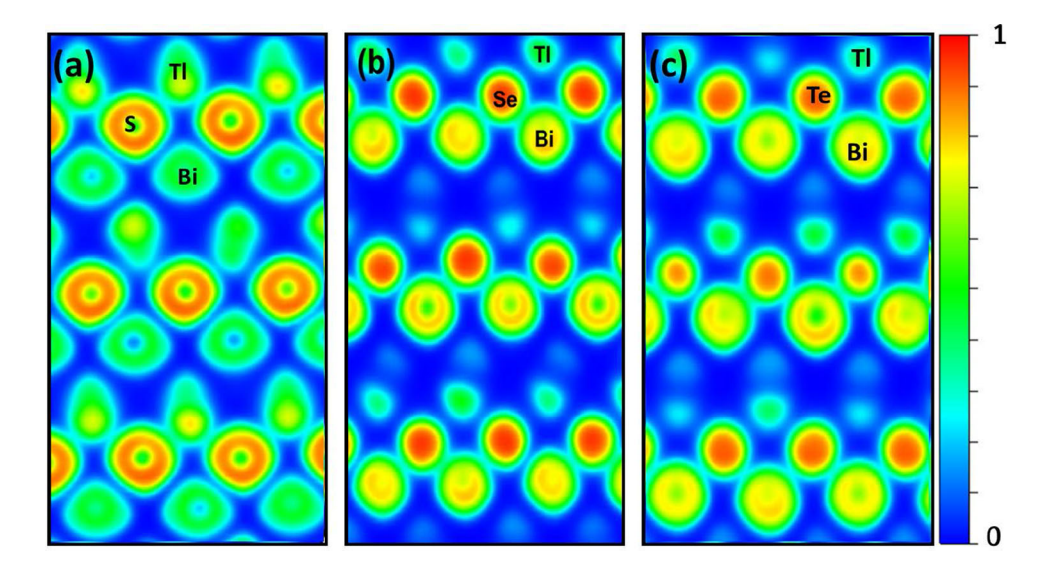


Table 3 Polarization in TlBiS₂, TlBiSe₂, and TlBiTe₂ in x, y, and z direction

Chalcopyrite materials	Polarization			
	x-Direction	y-Direction	z-Direction	
TlBiS ₂	8.56	8.55	8.71	
TlBiSe ₂	12.77	12.45	17.76	
$TlBiTe_2$	19.80	19.85	19.12	

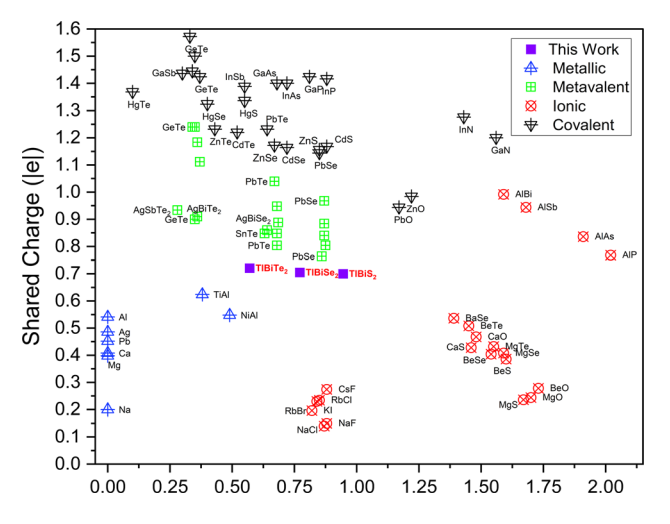


Figure 11 2-D map of shared electrons vs. transferred electrons of some representative materials. The materials studied in this work are represented by the purple color with red labels, and all of them are in the metavalent bonding region. Other data is taken from Ref. [47].

effective charges which also happen in CsSnBr₃ and CsPbBr₃ (both have lone-pair electrons) when compared to CsCaBr₃ that has no lone-pair electrons [59].

Correlation between strong phonon anharmonicity and metavalent bonding

Metavalent bonding occurs in all three materials discussed in this paper as confirmed by several descriptors [15, 16, 60]. The metavalent bonding is known for its pronounced phonon anharmonicity. A 2-D map of shared and transferred charges is the simplest descriptor to spot the location of the metavalent bonded materials [60]. A 2-D map shown by Fig. 11 of transferred vs shared electrons is used to show that all three chalcopyrite materials have metavalent bonding. One might argue that the type of interatomic bonding in the green region (metavalent bonding region) is still either covalent or metallic, but the unique descriptors of the metavalent bonding are distinctly different from the covalent and metallic bonds [15, 16, 60]. The unique descriptors of the metavalent bonds besides the 2-D map are moderate electronic conductivity, the unsatisfied 8-N rule in effective coordination number, high transverse optical Grüneisen parameter (> 3), high Born effective charges (usually 4-6), and high dielectric tensor (> 15) [15]. Those descriptors set the metavalent bonding apart from covalent, ionic, and metallic bonding types and make the metavalent bonding unique candidates for thermoelectrics and phase change materials [16]. The descriptors calculated in



Chalcopyrite materials	Born effective charges of Bi atom in x , y , and z directions	Dielectric constant	Grüneisen parameter of TO phonon mode
TlBiS ₂	6.39, 6.51, 5.40	15.00	6.270
TlBiSe ₂	6.75, 6.88, 5.59	22.04	7.706
TlBiTe ₂	7.70, 7.85, 6.58	25.43	6.623

Table 4 Computed Born effective charges of the central atom (Bi), dielectric constant, and the Grüneisen parameter of transverse optical (TO) phonon mode

this work are transverse optical Grüneisen parameter, Born effective charges, and dielectric tensor as shown in Table 4.

TlBiTe₂ seems to have the largest polarizability since it has the highest dielectric constant and Born effective charges of Bi (the central atom). The highest polarizability in TlBiTe₂ is due to the Te atoms having the largest atomic radius which causes higher repulsion with the lone-pair electrons in Tl and Bi and causes more polarization. The high values of dielectric constants and Born effective charges in TlBiS₂, TlBiSe₂, and TlBiTe₂ indicate that those materials have large LO-TO splitting [54] which is evidenced by the phonon dispersions in Figs. 4, 5 and 6. Metavalent bonded materials are known for their strong phonon anharmonicity. In fact, metavalent bonded chalcogenides are better thermoelectrics in terms of having higher thermoelectric figure of merit than chalcogenides with other types of bonds [16].

Conclusion

First-principles studies were carried out on TlBiS₂, TlBiSe₂, and TlBiTe₂, and their lattice thermal conductivities at 300 K were calculated using phonon Boltzmann transport equation. The lattice thermal conductivity differs in each direction, but the average thermal conductivity results are as follows: 0.8826 W/mK for TlBiS₂, 0.9383 W/mK for TlBiSe₂, and 0.2841 W/mK for TlBiTe₂. While TlBiTe₂ possesses the lowest lattice thermal conductivity, which is expected, the results demonstrate an anomalous trend in the lattice thermal conductivity of TlBiS₂ and TlBiSe₂. Unexpectedly, TlBiS₂ exhibits lower lattice thermal conductivity which contradicts with conventional Keyes' theory that indicates the inverse relation between mean atomic mass and lattice thermal conductivity with the same structure. Although most of the parameters of the lattice thermal conductivity such as volumetric heat capacity, group velocity, and phase space predict that TlBiS₂ would have higher lattice thermal conductivity, the anomalous behavior of the extremely short phonon relaxation time in TlBiS₂ especially in the optical phonon branches leads to a lower lattice thermal conductivity of TlBiS₂ than that of TlBiSe₂. We reveal that the anomalous behavior of phonon relaxation time in TlBiS₂ stems from the extensive strongly localized phonon modes solely associated with the vibrations of S atoms, which block the phonon transport in TlBiS₂, while in TlBiSe₂ and TlBiTe₂ the thermally conductive collective modes are present. Such strong phonon localization can be traced back to the high transferred charges in TlBiS₂ which consequently increases the phonon-phonon interactions. The ultralow lattice thermal conductivity in the three materials, regardless of the anomalous results between TlBiS₂ and TlBiSe₂, is due to the presence of the stereo-chemically lone-pair electrons which also induces large polarization in the materials as in other materials with lone-pair electrons, as evidenced by the large LO-TO splitting in the phonon dispersions. The presence of the metavalent bonding in these materials is confirmed by using various descriptors such as the position of the materials in the 2-D shared vs. transferred charges map, high transverse optical Grüneisen parameters, high Born effective charges, and high dielectric constants. The results gained in this study unravel a new physics about phonon transport anomaly in metavalent bonded materials which pave the way for designing novel materials for thermoelectric and thermal insulation applications.



Acknowledgements

Research reported in this publication was supported in part by the NSF (award number 2030128) and SC EPSCoR/IDeA Program under NSF OIA-1655740 via SC EPSCoR/IDeA SAN program (20-SA05). The support from National Natural Science Foundation of China [51720105007, 52076031, 51806031] and the computing resources from Supercomputer Center of Dalian University of Technology and the China National Grid (http://www.cngrid.org) / China Scientific Computing Grid (http://www.scgrid.cn) are greatly acknowledged.

Declarations

Declaration of interests The authors declare that they have no known competing financial interests or personal relationships that could have appeared to influence the work reported in this paper.

References

- [1] Fellet M (2018) Experiments confirm predicted high thermal conductivity of boron arsenide. MRS Bull 43(10):727–727
- [2] Tian F, Song B, Chen X, Ravichandran NK, Lv Y, Chen K, Sullivan S, Kim J, Zhou Y, Liu T-H et al (2018) Unusual high thermal conductivity in boron arsenide bulk crystals. Sci 361(6402):582–585
- [3] Dames C (2018) Ultrahigh thermal conductivity confirmed in boron arsenide. Sci 361(6402):549–550
- [4] Jana MK, Biswas K (2018) Crystalline solids with intrinsically low lattice thermal conductivity for thermoelectric energy conversion. ACS Energy Lett 3(6):1315–1324
- [5] Zhang X, Zhao L-D (2015) Thermoelectric materials: energy conversion between heat and electricity. J Materiomics 1(2):92–105
- [6] McGaughey AJH, Jain A, Kim H-Y (2019) Phonon properties and thermal conductivity from first principles, lattice dynamics, and the boltzmann transport equation. J Appl Phys 125(1):011101
- [7] Ma T, Chakraborty P, Guo X, Cao L, Wang Y (2019) First-principles modeling of thermal transport in materials: achievements, opportunities, and challenges. Int J Thermophys 41(1):9
- [8] Keyes RW (1959) High-temperature thermal conductivity of insulating crystals: relationship to the melting point. Phys Rev 115(3):564–567
- [9] Adachi S (2007) Lattice thermal conductivity of group-IV and III–V semiconductor alloys. J Appl Phys 102(6):063502

- [10] Yang Z, Yuan K, Meng J, Zhang X, Tang D, Hu M (2020) Why thermal conductivity of CaO is lower than that of CaS: a study from the perspective of phonon splitting of optical mode. Nanotechnology 32(2):025709
- [11] Valeri-Gil M, Rincón C (1993) Thermal conductivity of ternary chalcopyrite compounds. Mater Lett 17(1–2):59–62
- [12] Zhang Q, Cheng Y, Schwingenschlögl U (2015) Emergence of topological and topological crystalline phases in TlBiS₂ and TlSbS₂. Sci Rep 5(1):8379
- [13] Cava RJ, Ji H, Fuccillo MK, Gibson QD, Hor YS (2013) Crystal structure and chemistry of topological insulators. J Mater Chem C 1(19):3176
- [14] Ding G, Carrete J, Li W, Gao GY, Yao K (2016) Ultralow lattice thermal conductivity in topological insulator TlBiSe2. Appl Phys Lett 108(23):233902
- [15] Wuttig M, Deringer VL, Gonze X, Bichara C, Raty J-Y (2018) Incipient metals: functional materials with a unique bonding mechanism. Adv Mater 30(51):1803777
- [16] Yu Y, Cagnoni M, Cojocaru-Mirédin O, Wuttig M (2019) Chalcogenide thermoelectrics empowered by an unconventional bonding mechanism. Adv Funct Mater 30(8):1904862
- [17] Jain A, Ong SP, Hautier G, Chen W, Richards WD, Dacek S, Cholia S, Gunter D, Skinner D, Ceder G, Persson KA (2013) The materials project: a materials genome approach to accelerating materials innovation. APL Mater 1(1):011002
- [18] Kresse G, Furthmüller J (1996) Efficiency of Ab-Initio total energy calculations for metals and semiconductors using a plane-wave basis set. Comput Mater Sci 6(1):15–50
- [19] Kresse G, Furthmüller J (1996) Efficient iterative schemes forab initiototal-energy calculations using a plane-wave basis set. Phys Rev B 54(16):11169–11186
- [20] Kresse G, Joubert D (1999) From ultrasoft pseudopotentials to the projector augmented-wave method. Phys Rev B 59(3):1758–1775
- [21] Perdew JP, Burke K, Ernzerhof M (1996) Generalized gradient approximation made simple. Phys Rev Lett 77(18):3865–3868
- [22] Blöchl PE (1994) Projector augmented-wave method. Phys Rev B 50(24):17953–17979
- [23] Monkhorst HJ, Pack JD (1976) Special points for brillouinzone integrations. Phys Rev B 13(12):5188–5192
- [24] Manz TA, Limas NG (2016) Introducing DDEC6 atomic population analysis: part 1. Charge partitioning theory and methodology. RSC Adv 6(53):47771–47801
- [25] Limas NG, Manz TA (2016) Introducing DDEC6 atomic population analysis: part 2. Computed results for a wide range of periodic and nonperiodic materials. RSC Adv 6(51):45727–45747
- [26] Limas NG, Manz TA (2018) Introducing DDEC6 atomic population analysis: part 4. Efficient parallel computation of



- net atomic charges, atomic spin moments, bond orders, and more. RSC Adv 8(5):2678–2707
- [27] Togo A, Tanaka I (2015) First principles phonon calculations in materials science. Scr Mater 108:1–5
- [28] Li W, Carrete J, Katcho NA, Mingo N (2014) ShengBTE: a solver of the boltzmann transport equation for phonons. Comput Phys Commun 185(6):1747–1758
- [29] Wang H, Qin G, Li G, Wang Q, Hu M (2017) Low thermal conductivity of monolayer ZnO and its anomalous temperature dependence. Phys Chem Chem Phys 19(20):12882–12889
- [30] Yue S-Y, Qin G, Zhang X, Sheng X, Su G, Hu M (2017) Thermal transport in novel carbon allotropes with sp² or sp³ hybridization: An *Ab Initio* Study. Phys Rev B 95(8):085207
- [31] Zhou Y, Xiong S, Zhang X, Volz S, Hu M (2018) Author correction: thermal transport crossover from crystalline to partial-crystalline partial-liquid state. Nat Commun 9(1):4712
- [32] Qin G, Hu M (2018) Accelerating evaluation of converged lattice thermal conductivity. NPJ Comput Mater 4(1):3
- [33] Momma K, Izumi F (2011) VESTA 3for three-dimensional visualization of crystal, volumetric and morphology data. J Appl Crystallogr 44(6):1272–1276
- [34] Hinuma Y, Pizzi G, Kumagai Y, Oba F, Tanaka I (2017) Band structure diagram paths based on crystallography. Comput Mater Sci 128:140–184
- [35] Slack G (1973) Nonmetallic crystals with high thermal conductivity. J Phys Chem Solids 34(2):321–335
- [36] Lin S, Li W, Li S, Zhang X, Chen Z, Xu Y, Chen Y, Pei Y (2017) High thermoelectric performance of Ag9GaSe6 enabled by low cutoff frequency of acoustic phonons. Joule 1(4):816–830
- [37] Jiang B, Qiu P, Eikeland E, Chen H, Song Q, Ren D, Zhang T, Yang J, Iversen BB, Shi X et al (2017) Cu8GeSe6-based thermoelectric materials with an argyrodite structure. J Mater Chem C 5(4):943–952
- [38] Yao J, Takas NJ, Schliefert ML, Paprocki DS, Blanchard PER, Gou H, Mar A, Exstrom CL, Darveau SA, Poudeu PFP et al (2011) Thermoelectric Properties Ofp-Type CuInSe2chalcopyrites Enhanced by Introduction of Manganese. Phys Rev B 84(7):075203
- [39] Pan S, Wang C, Zhang Q, Yang B, Cao Y, Liu L, Jiang Y, You L, Guo K, Zhang J et al (2019) A₂Cu₃In₃Te₈ (A = Cd, Zn, Mn, Mg): a type of thermoelectric material with complex diamond-like structure and low lattice thermal conductivities. ACS Appl Energy Mater 2(12):8956–8965
- [40] Rashkeev SN, Lambrecht WRL (2001) Second-harmonic generation of I-III-VI2chalcopyrite semiconductors: effects of chemical substitutions. Phys Rev B 63(16):165212

- [41] Ouyang T, Liu Q, Chen M, Tang C, Li J, Zhang C, He C, Bao H, Zhong J, Hu M (2018) Doping induced abnormal contraction and significant reduction of lattice thermal conductivity of open framework Si24. ES Energy Environ 3:88–95
- [42] Zhao Y, Al-Fahdi M, Hu M, Siriwardane EMD, Song Y, Nasiri A, Hu J (2021) High-throughput discovery of novel cubic crystal materials using deep generative neural networks. Adv. Sci, 2100566.
- [43] Al-Fahdi M, Rodriguez A, Ouyang T, Hu M (2021) Highthroughput computation of new carbon allotropes with diverse hybridization and ultrahigh hardness. Crystals 11:783
- [44] Chakraborty P, Xiong G, Cao L, Wang Y (2018) Lattice thermal transport in superhard hexagonal diamond and wurtzite boron nitride: a comparative study with cubic diamond and cubic boron nitride. Carbon 139:85–93
- [45] Lindsay L (2016) First principles peierls-boltzmann phonon thermal transport: a topical review. Nanoscale Microscale Thermophys Eng 20(2):67–84
- [46] Qi J, Chen X, Yu W, Cadden-Zimansky P, Smirnov D, Tolk NH, Miotkowski I, Cao H, Chen YP, Wu Y et al (2010) Ultrafast carrier and phonon dynamics in Bi₂Se₃ Crystals. Appl Phys Lett 97(18):182102
- [47] Lindsay L, Broido DA (2008) Three-Phonon phase space and lattice thermal conductivity in semiconductors. J Phys Condens Matter 20(16):165209
- [48] Okubo K, Tamura S-I (1983) Two-phonon density of states and anharmonic decay of large-wave-vector LA phonons. Phys Rev B 28(8):4847–4850
- [49] Peng B, Zhang H, Shao H, Xu Y, Zhang X, Zhu H (2016) Low lattice thermal conductivity of stanene. Sci Rep 6(1):20225
- [50] Wang FQ, Hu M, Wang Q (2019) Ultrahigh thermal conductivity of carbon allotropes with correlations with the scaled pugh ratio. J Mater Chem A 7(11):6259–6266
- [51] Dugdale JS, Macdonald DKC (1955) Lattice thermal conductivity. PhySH 98:1751–1752
- [52] Cammarata A, Polcar T (2021) Fine control of lattice thermal conductivity in low-dimensional materials. Phys Rev B 103(3):035406
- [53] Elalfy L, Music D, Hu M (2021) metavalent bonding induced abnormal phonon transport in diamondlike structures: beyond conventional theory. Phys Rev B 103(7):075203
- [54] Skoug EJ, Morelli DT (2011) Role of lone-pair electrons in producing minimum thermal conductivity in nitrogen-group chalcogenide compounds. Phys Rev Lett 107(23):235901
- [55] Qin G, Qin Z, Wang H, Hu M (2018) Lone-pair electrons induced anomalous enhancement of thermal transport in



- strained planar two-dimensional materials. Nano Energy 50:425-430
- [56] Lee S, Esfarjani K, Luo T, Zhou J, Tian Z, Chen G (2014) Resonant bonding leads to low lattice thermal conductivity. Nat Commun 5(1):3525
- [57] Albanesi EA, Okoye CMI, Rodriguez CO, Blanca ELPY, Petukhov AG (2000) Electronic structure, structural properties, and dielectric functions of IV-VI semiconductors: PbSe and PbTe. Phys Rev B 61(24):16589–16595
- [58] Fabini DH, Seshadri R, Kanatzidis MG (2020) The underappreciated lone pair in halide perovskites underpins their unusual properties. MRS Bull 45(6):467–477
- [59] Fabini DH, Laurita G, Bechtel JS, Stoumpos CC, Evans HA, Kontos AG, Raptis YS, Falaras P, Ven AVD, Kanatzidis MG et al (2016) Dynamic Stereochemical Activity of the Sn²⁺ Lone Pair in Perovskite CsSnBr₃. J Am Chem Soc 138(36):11820–11832
- [60] Raty JY, Schumacher M, Golub P, Deringer VL, Gatti C, Wuttig M (2018) A quantum-mechanical map for bonding and properties in solids. Adv Mat 31(3):1806280

Publisher's Note Springer Nature remains neutral with regard to jurisdictional claims in published maps and institutional affiliations.

